Earth and Planetary Science Letters 426 (2015) 259–266

Contents lists available at ScienceDirect

Earth and Planetary Science Letters

www.elsevier.com/locate/epsl

Constraining the age of Liuqu Conglomerate, southern Tibet: Implications for evolution of the India–Asia collision zone

Guangwei Li [a,*], Barry Kohn [a], Mike Sandiford [a], Zhiqin Xu [b], Lijie Wei [c]

[a] School of Earth Sciences, The University of Melbourne, Parkville, Victoria 3010, Australia
[b] State Laboratory for Continental Tectonics and Dynamics, Institute of Geology, Chinese Academy of Geological Sciences, Beijing 100037, China
[c] Institute of Geomechanics, Chinese Academy of Geological Sciences, Beijing 100081, China

ARTICLE INFO

Article history:
Received 25 February 2015
Received in revised form 26 May 2015
Accepted 3 June 2015
Available online 25 June 2015
Editor: A. Yin

Keywords:
low temperature thermochronology
Liuqu conglomerate
Indus–Yarlung suture zone
Tibetan plateau

ABSTRACT

Controversy over the depositional age and provenance of the Liuqu Conglomerate along the major structural Indus–Yarlung suture zone in South Tibet clouds our understanding of the process of the India/Asia collision. Here, we report low-temperature thermochronometric data (apatite fission track, apatite and zircon (U–Th)/He for the Liuqu Conglomerate in the Xigaze area). Our new data constrain its depositional age to latest Oligocene–Early Miocene time, indicating that rather than having formed immediately following Paleogene India–Asia collision or collision between India and an intra-oceanic arc as previously proposed, the Conglomerate was probably deposited in an intermontane basin, at a slightly later time than the Gangrinboche Group to the north. The Liuqu Conglomerate should therefore not be used as a key horizon in models constraining the early stages of India/Asia collision. Our data together with previous studies suggest that the Liuqu Conglomerate was sourced from the Xigaze forearc basin, Indus–Yarlung suture zone, as well as the Tethyan Himalaya. Furthermore, our data indicate that exhumation of the Liuqu Conglomerate commenced at ~<10–12 Ma, suggesting significant erosion in the Indus–Yarlung suture zone attributable to incision of the Yarlung Zangbo in Mid to Late Miocene time.
© 2015 Elsevier B.V. All rights reserved.

1. Introduction

Convergence of the Indian and Asian plates resulted in the closure of Neotethys and ultimately the uplift of the Himalayan–Tibetan orogen (e.g. Allégre et al., 1984; Harrison et al., 1992). The remnants of syn-orogenic deposits in southern Tibet contain some of the most important archives of these events (Ding et al., 2005; DeCelles et al., 2011), relevant to both the timing and the palaeogeography of early stage collision. Two distinct clastic sedimentary groups have been recognized along the Indus–Yarlung suture zone, on either side of the Indus–Yarlung ophiolite (Aitchison et al., 2002; Davis et al., 2002; Ding et al., 2005; Fang et al., 2006; DeCelles et al., 2011). On the northern side, the sediments include the Paleocene Tso-jiangding deposits (Ding et al., 2005; Hu et al., 2015) and the Upper Oligocene–Miocene Gangrinboche Conglomerates (Aitchison et al., 2002; DeCelles et al., 2011; Fig. 1). While on the southern side, the Cenozoic sedimentary rocks include the Middle Paleogene to Lower Eocene Sangdanlin–Zheya Formations (Ding et al., 2005; Wan et al., 2007) and terrestrial Liuqu Conglomerate (David et al., 2002; Fang et al., 2006; Fig. 1).

The depositional environment of the Liuqu Conglomerate has been attributed to markedly different tectonic settings and because its age is uncertain, it is arguably one of the most debated units in studies of the geological evolution of southern Tibet. It is widely considered as a molasse (or proximal foreland basin) unit deposited immediately following initial India–Asia collision in the Paleocene (e.g. Fang et al., 2006; J.G. Wang et al., 2010; DeCelles et al., 2011; Wei et al., 2011). Aitchison et al. (2007) however, consider that collision occurred between India and an intra-oceanic arc during the Eocene, prior to the main India–Asian collision *sensu-stricto*, although this view is disputed widely (e.g. Najman et al., 2010; DeCelles et al., 2014; references therein). Based on plant impressions, its depositional age has been assigned variously to: Late Cretaceous (Guo, 1975), Middle to Late Eocene (Tao, 1998; Fang et al., 2006) or Late Eocene–Miocene (Yin et al., 1988). On the basis of stratigraphic relationships, Davis et al. (2002) inferred that the Liuqu Conglomerate was deposited in the Paleogene. J.G. Wang et al. (2010) reported Palaeocene detrital zircons from the conglomerate, while two detrital zircons yielding a U–Pb age of ca. 18 Ma were reported by Leary et al. (2013), suggesting a Neogene depositional age. Furthermore, Davis et al. (2002) suggested that the Liuqu Conglomerate was sourced from both the Indus–Yarlung suture zone to the north and from Tethyan Himalaya to

* Corresponding author. Tel.: +61 3 90357571; fax: +61 3 83447761.
E-mail address: guangwei.li@unimelb.edu.au (G. Li).

http://dx.doi.org/10.1016/j.epsl.2015.06.010
0012-821X/© 2015 Elsevier B.V. All rights reserved.

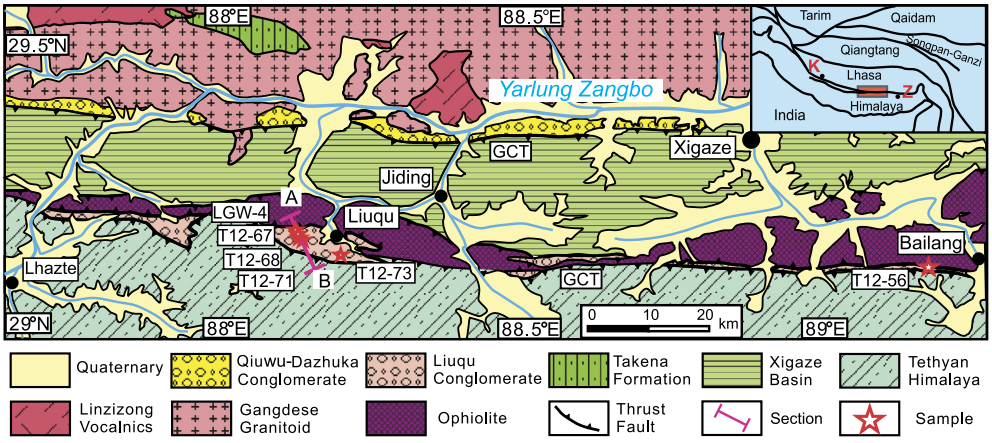

Fig. 1. Red inset showing study area. Simplified geological map of Xigaze region, South Tibet and cross section line (A–B) in Liuqu area showing positions of samples. GCT = Great Counter Thrusts; TH = Tethyan Himalaya; K = Kailas; Z = Zedang. (For interpretation of the references to color in this figure legend, the reader is referred to the web version of this article.)

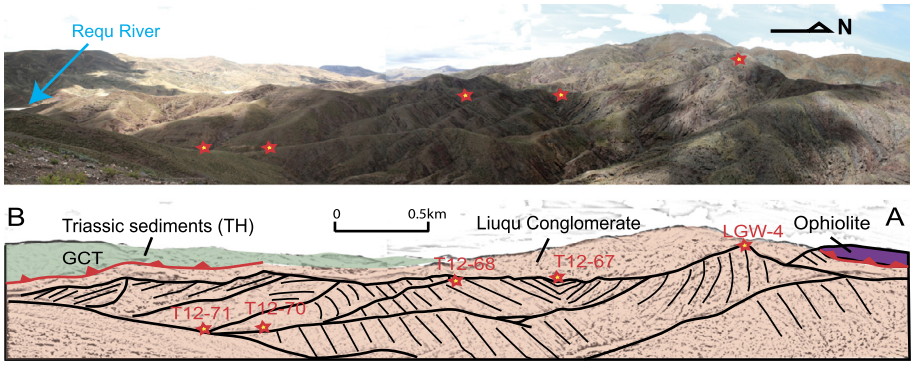

Fig. 2. Panoramic view looking westward from a ridge near Liuqu township. Liuqu Conglomerate is well exposed in a section showing a syncline and anticline. The view covers the cross section (A–B) in Liuqu area (Fig. 1) showing locations of main samples (see abbreviations in Fig. 1).

the south (Fig. 1), while J.G. Wang et al. (2010) and Leary et al. (2013) proposed an exclusive provenance from the Xigaze forearc basin to the north. Several constraints provide a minimum depositional age for the Liuqu Conglomerate. The Great Counter Thrust (GCT), which mainly defines its southern boundary (Figs. 1, 2), was active between ~19–15 Ma in the Zedang (Quidelleur et al., 1997) and ceased at ~17–16 Ma in the Kailas (DeCelles et al., 2011; Carrapa et al., 2014). In addition, a dike cutting the basal Liuqu Conglomerate in the study area provides a minimum depositional age of ca. 20 Ma (Leary et al., 2013).

Over the past two decades, the low-temperature (low-T) thermochronology has been widely used to reconstruct sedimentary basin evolution including provenance, burial history and exhumation processes (e.g. Garver et al., 1999; Armstrong, 2005). Low-T thermochronology data make it possible to constrain thermal histories over particular temperature ranges; for example, the partial He retention zones of the AHe and ZHe system are ~40–80 °C and ~130–200 °C, respectively (e.g. Farley, 2002; Reiners et al., 2004; Wolfe and Stockli, 2010), while the AFT partial annealing zone is typically between ~60–110 °C (Gleadow et al., 2002). Additionally, if detrital cooling ages are older than the depositional age, they probably represent a sediment source thermal history signal; on the other hand, if detrital cooling ages are younger than the depositional age of the host strata, they indicate post-depositional thermal resetting.

Hence, we report a low-temperature thermochronology apatite fission track (AFT), apatite and zircon U-Th/He (AHe and ZHe) data from detrital grains, to further constrain the depositional history of the Liuqu Conglomerate. In confirming multiple provenances feeding a Neogene depositional process following juxtaposition of both Asian and Indian sources, our new data help resolve key aspects of this controversy, and provide new constraints on the uplift/exhumation of the India–Asia collision zone in southern Tibet.

2. Study area and samples

The Indus–Yarlung suture zone represents remnants of the Neo-Tethys oceanic basin, which in south Tibet marks the boundary between Indian and Asian continents in south Tibet (e.g. Gansser, 1964; Allégre et al., 1984; Yin, 2006). It juxtaposes the Lhasa terrane (e.g. Xigaze Basin and Gangdese Belt) to the north and the Tethyan Himalayan to the south (Yin, 2006; Fig. 1). The Liuqu Conglomerate, structurally the uppermost unit within the Indus–Yarlung suture zone, crops out discontinuously from Lhaze to Bainang, extending for more than 150 km from west to east with outcrop widths varying between hundreds of metres to kilometres (Fig. 1). The outcrops studied here occur between the towns of Liuqu and Bailang, near Xigaze. Here, the Liuqu Conglomerate unconformably outcrops between the Indus–Yarlung ophiolite to the north and the Mesozoic low-grade metasedimentary rocks of the Tethyan Himalayan sequences to the south (Yin, 2006), in an open east–west trending, asymmetrical syncline and anticline pair (Fig. 2). The boundaries of the Liuqu Conglomerate are defined by the GCT. The Liuqu Conglomerate is composed predominantly of mottled and purple reddish sandy conglomerates, as well as reddish sandstone intercalated with grey–green and reddish muddy sandstones and silty mudstones (Figs. 3 and 4) inferred to have been deposited in a transitional alluvial fan or braided river environment (Davis et al., 2002).

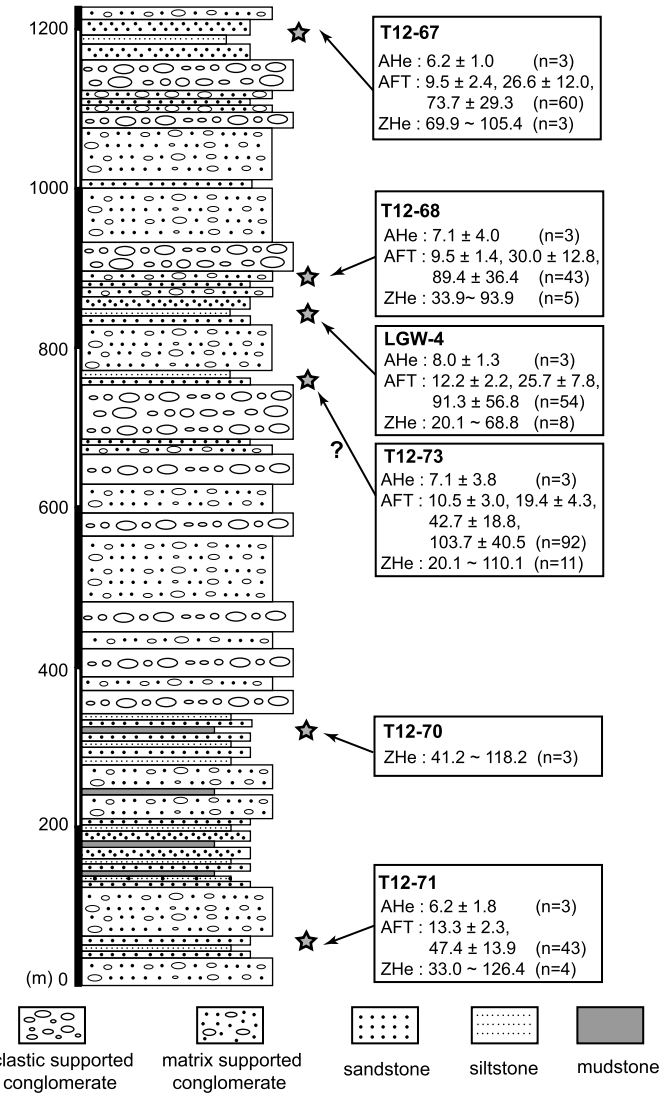

Fig. 3. Generalized stratigraphic column of the Liuqu Conglomerate showing location of samples and their low temperature thermochronology data.

We collected six sandstone samples from the Liuqu area, and another one from the Bailang area (Figs. 1–4). These samples were collected over a restricted range of elevation from 4000 to 4500 m (Table 1). Detrital-grain ages and cooling histories were obtained using low-T thermochronology (AHe, AFT, and ZHe dating).

3. Methods

3.1. Apatite fission track (AFT) analysis

Apatite grains were mounted in epoxy resin on glass slides, ground and polished to an optical finish to expose internal grain surfaces. Polished mounts were etched in 5M HNO_3 for 20 s at 20 °C to reveal the fossil tracks. Using a vacuum unit, a gold coating (~5–7 nm thickness) was applied to the etched mounts so as to enhance the reflectivity of the polished surface, and minimize internal reflections under the microscope (Gleadow et al., 2009). Apatite grains with polished surfaces parallel to prismatic crystal faces and homogeneous track distributions were selected using a Zeiss Axio Imager M1m microscope. Stacks of high-resolution digital images of each selected grain were then captured under both transmitted and reflected light using a Zeiss camera at a total magnification of ×1000 under both transmitted and reflected light. The pixel-size (~0.0698–0.0705 μm/pixel) of the images was precisely calibrated. Track counting was performed using the coincidence mapping protocol (Gleadow et al., 2009). Uranium measurements of selected grains were carried out using an Agilent 7700 LA-ICP-MS (Laser Ablation Inductively Coupled Plasma Mass Spectrometer) (Hasebe et al., 2004). Using a New Wave UP-213 laser, ablation was carried out (30 μm diameter beam size, ~2.0 J/cm^2 energy and 5 Hz repetition rate), over 25 s on selected grains, and calibration standards NIST-612 glass and apatite Mud Tank (uranium-content calibration standard). Etch pit diameters (*Dpar*) of grains from which tracks were counted were also determined (see supplementary data). Additionally, low spontaneous track densities in most apatite grains (due largely to their low uranium content and in some cases their relatively young age) preclude the availability of tracks for length measurement.

The distribution probability of AFT grain ages was determined using the Binomfit program (Brandon, 1996). Radial plots were also used for analysing the distribution of the detrital AFT ages and similar age peaks for all samples are plotted in Fig. 5.

3.2. Apatite electron microprobe analysis

Apatite halogen content was analysed using a Cameca SX50 Electron Microprobe using a wavelength-dispersive (WDS) method that employed TAP, PET, and LIF crystals with 2 mm spatial resolution, 15 kV beam conditions and 35 nA beam current. For analysis of apatites, an electron beam of 10 um diameter with an accelerating voltage of 15 kV and a beam current of 35 nA was used. Analytical precision for most elements is <1%, but was ~5% for F and Cl.

3.3. Apatite and zircon (U–Th)/He analysis

For (U–Th)/He analysis apatite and zircon grains were immersed in ethanol and examined under polarised light to detect possible mineral inclusions. Only clear and euhedral grains were selected for analysis. Digitised photographs were taken for calculation of the alpha correction factor (F_T; e.g. Farley et al., 1996). Protocols for He analysis followed an established laboratory routine for laser He extraction (House et al., 2002). Apatite and zircon samples were loaded into platinum tubes and outgassed under vacuum at ~900 °C for 5 min and ~1300 °C for 15 min respectively, using a fibre-optically coupled diode laser with a 820 nm wavelength. ^{4}He abundances were determined by isotope dilution using a ^{3}He spike, calibrated against an independent ^{4}He standard. The uncertainty in the sample ^{4}He measurement is estimated at <1%. Apatite U–Th–Sm data were acquired via total dissolution of the outgassed apatite Pt tubes in HNO_3 and analysed using an Agilent 7700 ICP-MS. For zircon determination of U and Th content grains were removed from their Pt tubes and transferred to Parr bombs where they were spiked with ^{235}U and ^{230}Th and digested at 240 °C for 40 h in HF. Standard solutions containing the same amount of spike as samples were treated identically, as were a series of unspiked reagent blanks. A second bombing in HCl for 24 h at 200 °C ensured dissolution of fluoride salts and final solutions were diluted to 10% acidity for analysis on an Agilent 7700 ICP-MS. Analytical uncertainties for the University of Melbourne (U–Th)/He facility are conservatively assessed to be ~6.2% ($\pm 1\sigma$), which incorporates the α-correction-related constituent and takes into account an estimated 5 μm uncertainty in grain size measurements, gas analysis and ICP-MS uncertainties. Durango apatite and Fish Canyon Tuff zircon were run as an internal standard with each batch of samples analysed and served as an additional check on analytical accuracy.

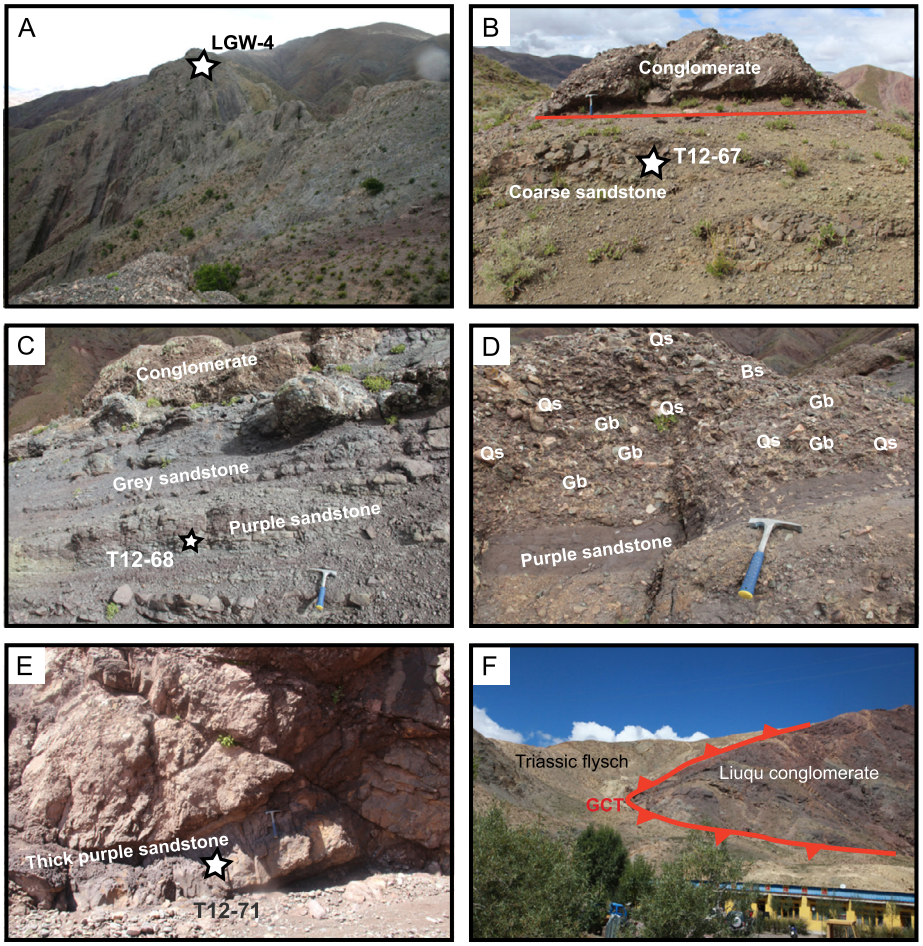

Fig. 4. Field features and lithologies of the Liuqu Conglomerate. A, vertical northern limb of syncline in the Liuqu section; B. core of syncline in the Liuqu section; C. southern limb of syncline near the core of the anticline; D. pebbles in the Liuqu Conglomerate, including Qs – quartz schist, Bs – Basalt, Gb – Gabbro, etc.; E. location of purple sandstone sample T12-71 near base of Liuqu Conglomerate; F. southernmost Liuqu section, showing Triassic sediments (Tethyan Himalaya) thrust over the Liuqu Conglomerate.

Table 1
Thermochronological age data for the Liuqu Conglomerate.

Sample number	(U–Th–Sm)/He apatite[a,b] (Ma)	(U–Th)/He zircon[c] (Ma)	Age peaks apatite fission track[d] (Ma)			
			P1 (~10)	P2 (~20)	P3 (~30–40)	P4 (~70–90)
T12-56			–	16.6 ± 3.7	28.6 ± 3.2	64.0 ± 16
T12-67	6.2 ± 1.0	69.9 ~ 105.4	9.5 ± 2.4	26.6 ± 12.0	–	73.7 ± 29.3
T12-68	7.1 ± 2.4	33.9 ~ 93.9	9.5 ± 1.4	–	30.0 ± 12.8	89.4 ± 36.4
T12-71	6.2 ± 1.8	33.0 ~ 126.4	13.3 ± 2.3	–	47.4 ± 13.9	–
T12-73	7.1 ± 1.9	20.1 ~ 110.1	10.5 ± 3.0	19.4 ± 4.3	42.7 ± 18.8	103.7 ± 40.5
LGW-4	8.0 ± 1.3	20.1 ~ 68.8	12.2 ± 2.2	25.7 ± 7.8	–	91.3 ± 56.8
Total peaks	6.8 ± 1.3	20, 33, 47, 65, 103	11.5 ± 1.2	24.5 ± 2.6	46.4 ± 7.4	87.5 ± 17.0
AFT (<0.2) peak[e]				10.8 ± 1.0		
AFT (>0.2) peaks[e]				14.5 ± 2.1, 32.1 ± 5.9, 76.3 ± 12.7		

[a] Reported error limits are $\pm 1\sigma$;
[b] Weighted mean age calculated using Isoplot 3.0 (Ludwig, 2003);
[c] Age peaks calculated using Isoplot 3.0 (Ludwig, 2003);
[d] Age peaks calculated using Binomfit (Brandon, 1996);
[e] AFT age peaks for detrital apatite grains with Cl (wt%) < 0.2 or >0.2.

4. Results

In total, the samples yielded five weighted mean AHe ages each of which was calculated from three single grans, six groups of detrital AFT ages (364 grains) and six groups of detrital ZHe ages (34 grains) (Table 1; Fig. 3; see supplementary data). Probabilities of detrital AFT ages were calculated using BinomFit for AFT ages (Brandon, 1996) and the probability densities of ZHe ages using Isoplot (Ludwig, 2003).

4.1. Detrital AFT ages and halogen composition of detrital apatite grains

Dispersed single-grain AFT ages of six samples range from ~140 to 5 Ma, with four age-peaks of ~10, 20, 30–40 and

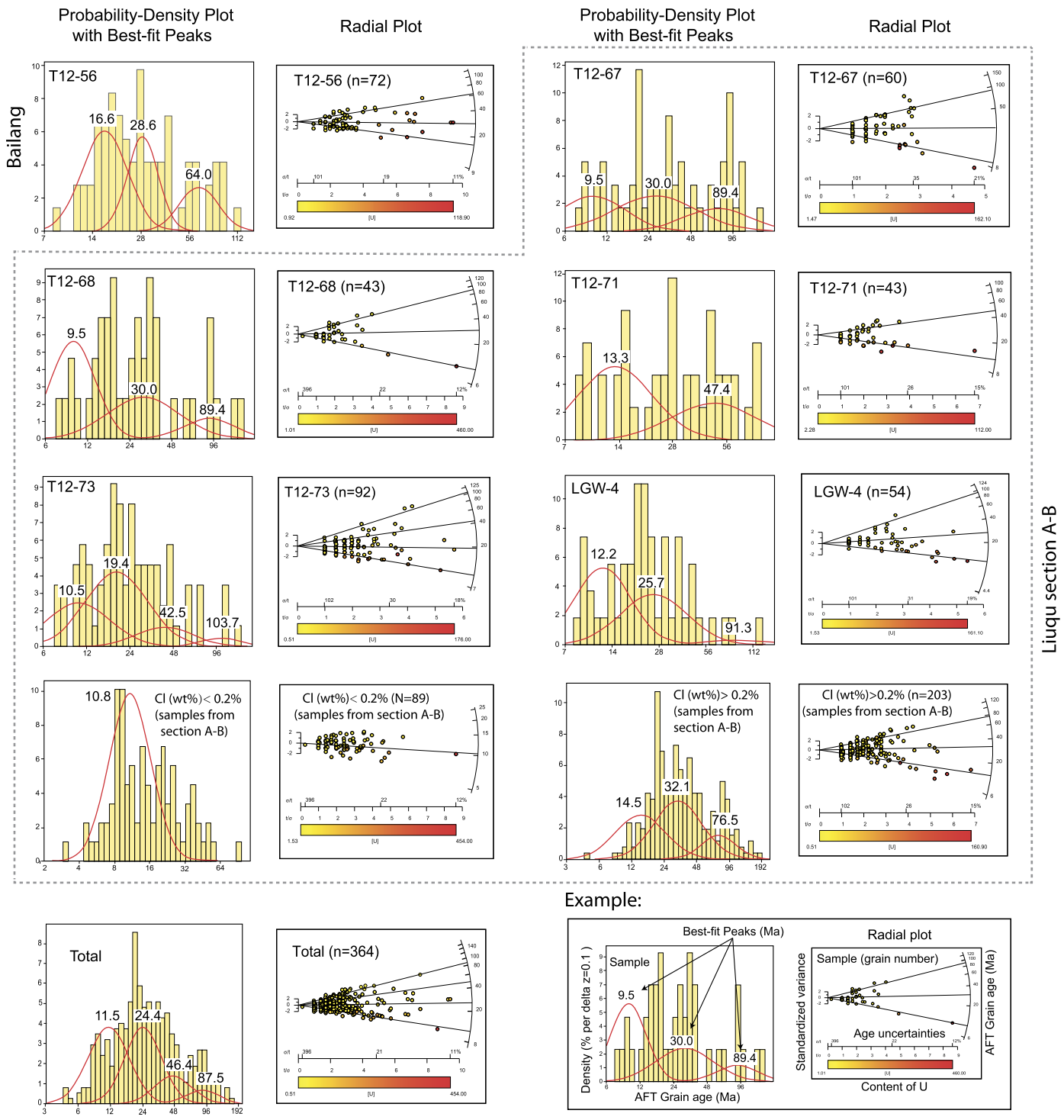

Fig. 5. AFT age probability distributions of detrital apatites from the Liuqu Conglomerate and plots with individual grain ages (using Binomfit, Brandon, 1996). Red lines are 'fitting' curves. Cl (wt%) <0.2 = grains with Cl (wt%) <0.2 and Cl (wt%) <0.2 = grains with Cl (wt%) >0.2 in Liuqu area (section A–B in Fig. 1); Total = all grains in this study. *Note:* Green et al. (1985) reported a variation of single grain apatite Cl content versus fission track age, which demonstrates the preferential retention of tracks in Cl-rich apatites. In that study, ages of those grains with ~0.2 Cl (wt%) were almost or completely reset to about ~0 Ma at ~92 °C. Assuming similar conditions for this study, we adopted a value of 0.2 Cl (wt%) for dividing the detrital apatite grain population into two groupings, reflecting their variable temperature sensitivities. (For interpretation of the references to color in this figure legend, the reader is referred to the web version of this article.)

70–90 Ma (Table 1 and Fig. 5). Cl and F content (wt%) of detrital apatite grains are distributed over a wide range of 1.68–5.36% and 0–1.86%, respectively (see supplementary data).

Given that resistance to track annealing in apatite increases with greater Cl content (wt%) (e.g. Green et al., 1985; Burtner et al., 1994), we divided the single grain AFT ages of five samples from Liuqu area (section A–B, Figs. 1 and 2) into two groups, one including grains with <0.2 Cl (wt%) content and another with grains >0.2 Cl (wt%) (Fig. 5). We calculated a single peak at 10.8 ± 1.0 Ma for grains with <0.2 Cl (wt%) representing those grains with the lowest temperature annealing sensitivity, while the other group including the higher annealing sensitivity grains yielded three age-peaks of 14.5 ± 2.1, 32.1 ± 5.9 and 76.3 ± 12.7 Ma (Table 1 and Fig. 5).

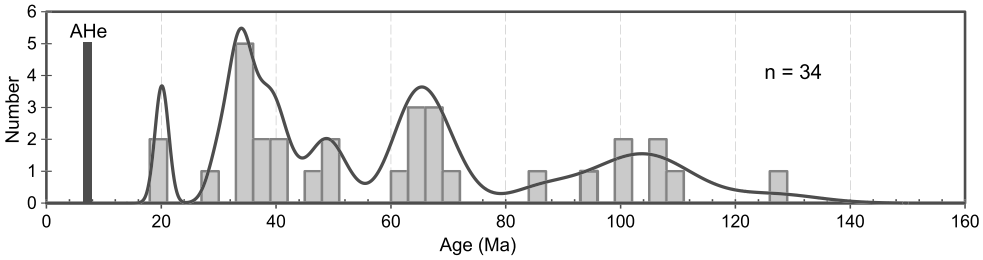

Fig. 6. Probability distribution of zircon (U–Th)/He ages from the Liuqu Conglomerate, calculated using Isoplot (Ludwig, 2003), showing four peaks of ~20, 37, 66 and 104 Ma, with a minor peak at 47 Ma.

Sample T12-56 from the Bailang area ~80 km east of Liuqu area, yields three age peaks of 16.6 ± 3.7, 28.6 ± 3.2, and 64.0 ± 16 Ma, which are slightly older than those from section A–B (Fig. 5).

4.2. AHe and ZHe ages

The five samples from the Liuqu area yield consistent AHe ages between ~6–8 Ma (Table 1 and supplementary data). They are much younger than the minimum limit of its depositional age, indicating these AHe ages have been thermally reset.

Four groups of detrital ZHe ages, including 34 scattered single grain ages in the range of ~126.4–20.1 Ma (Table 1 and supplementary data), yielded four main age peaks of ~20, 33, 65 and 103 Ma, as well as a minor peak of ~47 Ma (Fig. 6).

5. Discussion

5.1. Depositional age of Liuqu Conglomerate

The AHe age range of ~6–8 Ma is significantly younger than the minimum bounds on deposition cited earlier (e.g. Leary et al., 2013). As such the AHe data imply complete post-depositional thermal resetting with peak burial temperatures exceeding ~80 °C. By contrast, AFT and ZHe ages are dispersed with multi-peak distributions and age ranges that extend beyond plausible maximum depositional ages.

For the AFT system we interpret the ages as indicative of incomplete post-depositional thermal resetting, implying maximum burial temperatures of less than ~110 °C (see also Fig. 5). Those apatites with a value <0.2 Cl (wt%) from samples in the Liuqu area yield AFT ages at a peak of 10.8 ± 1.0 Ma which reflect cooling from temperatures where such grains have been almost or totally annealed, thereby probably indicating the timing of regional erosion/or local incision. We estimate this temperature to be ~90 ± 5 °C and this would be consistent with the fact that coexisting AHe ages indicate that they have cooled from temperatures >~80 °C (i.e. from a temperature higher than the upper temperature limit of the nominal He partial retention zone). The ages of the other group with >0.2 Cl (wt%) probably reflect partially annealed ages (Green et al., 1985). Furthermore, this heating of the conglomerate can probably be attributed to the post-depositional structural burial (Fig. 4F) and deformation (Fig. 2) related to movement of the GCT (Figs. 1 and 2).

Because such temperatures are too low to reset the ZHe system, ZHe ages are interpreted as only preserving provenance signatures. As such the youngest ZHe age of ~20.1 Ma from the upper part of the Liuqu Conglomerate, is considered to provide a constraint on the maximum depositional age of its upper part. Additionally, the peak of apparent AFT ages of grains with <0.2 Cl (wt%) at ~10.8 ± 1.0 Ma is interpreted to reflect significant post depositional resetting, while AFT age peaks for grains with >0.2 Cl (wt%) represent the partially annealed provenance ages. Hence, the depositional age of the Liuqu Conglomerate was older than the youngest peak of 10.8 ± 1.0 Ma from grains with <0.2 Cl (wt%). Furthermore, considering the timing of termination of GCT movement in the region, which constrains the boundary of the conglomerate (Quidelleur et al., 1997; Carrapa et al., 2014), we suggest that its depositional age should at least be older than ~15 Ma. We therefore consider that the upper part of Liuqu conglomerate was deposited between ~20 Ma and ~15–16 Ma.

For the lower part of the Liuqu Conglomerate, we note that the youngest ZHe age reported here from the base of the Liuqu Conglomerate is ~33 Ma, allowing the possibility that deposition may have commenced as early as Oligocene. This would be consistent with the 20 Ma age of a dike cutting the basal Liuqu Conglomerate (Leary et al., 2013). Thus, the depositional age of the entire Liuqu Conglomerate could be constrained into a time span of ~33 to ~15 Ma. However, given the rapid depositional characteristics of the Liuqu Conglomerate (Davis et al., 2002), its depositional age is probably Early Miocene. Based on the discussion above, the Liuqu Conglomerate is therefore probably younger than the Qiuwu-Dazhuka conglomerates (which are belong to the upper Oligocene–Lower Miocene Gangrinboche/Kailas Group) to the north (Aitchison et al., 2002; DeCelles et al., 2011; Wang et al., 2013).

5.2. Provenance of Liuqu Conglomerate

Apparent AFT ages yield three different partially annealed age peaks, at ~15–20, 30–40 and 70–90 Ma, while ZHe ages (but with less data) show five peaks at ~20, 33, 47, 65 and 103 Ma (Table 1 and Figs. 3, 6). Low-temperature thermochronology data available from neighbouring terranes may also help to interpret these ages. For example, AFT and ZHe ages from Tethyan Himalaya (Najman et al., 2010; Li et al., 2015) and the Greater Himalaya (e.g. van der Beek et al., 2009; A. Wang et al., 2010) to the south are exclusively Cenozoic in age. By contrast, AFT data from the Xigaze forearc basin (age range of ~20–70 Ma, our unpublished data), and AFT and ZHe data from the Lhasa and Qiangtang terranes both include populations of Cretaceous–Cenozoic age (e.g. Hetzel et al., 2011; Rohrmann et al., 2012; Dai et al., 2013). Thus we conclude that pre-Cenozoic grains of the Liuqu Conglomerate were probably derived from terranes to the north, especially the Xigaze forearc basin. This is in agreement with suggestions by J.G. Wang et al. (2010) and Leary et al. (2013) based on U–Pb ages of detrital zircons. Further, the Liuqu Conglomerate, characterised by its coarse-grained and immature sedimentary features (Figs. 3 and 4; Davis et al., 2002), clearly had proximal sources. According to detailed petrography of the Liuqu Conglomerate described by Davis et al. (2002) and J.G. Wang et al. (2010), the Indus–Yarlung suture zone provided clasts of basalt, gabbro, serpentinite and radiolarian chert to the Liuqu Conglomerate (Fig. 2), while the Tethyan Himalaya, which lies immediately south of the conglomerate and includes typical components (quartz–arenite, slate, and phyllite), also supplied such clasts to the

conglomerate. Combined with previous studies (Davis et al., 2002; J.G. Wang et al., 2010), we suggest that the Liuqu Conglomerate was derived from the Indus–Yarlung suture zone, Xigaze forearc basin, as well as the Tethyan Himalaya.

5.3. Incision along the Indus–Yarlung suture zone

The reset peak for detrital AFT ages of grains with <0.2 Cl (wt%) at ~10.8 ± 1.0 Ma from the six samples in section A–B (Figs. 1–3; Table 1), is generally consistent with data reported from the Zedang area (Li et al., 2015) along the Indus–Yarlung suture zone, which probably represent post-depositional/thrust cooling ages. However, it is worth noting that exhumation of the Liuqu Conglomerate and sedimentary rocks in the Zedang area is slightly younger than that of the Gangrinboche Group in the Kailas (~16 Ma) which is located on the north side of the Indus–Yarlung suture zone (Fig. 1). This suggests possible southward migration of exhumation along the Indus–Yarlung suture zone. Combined with the younger Late Miocene AHe ages (~6–8 Ma) from the Liuqu Conglomerate (Table 1), these results suggest rapid post Early Miocene exhumation of the Indus–Yarlung suture zone until ~6–8 Ma, which was probably facilitated by incision of the Yarlung Zangbo (Fig. 1). Our data also support the proposition that significant removal of material from the Indus–Yarlung region along the Yarlung Zangbo occurred over a time-span of a few million years (Carrapa et al., 2014). This is supported by a pronounced increase of oceanic $^{87}Sr/^{86}Sr$ ratios in Late Miocene time (e.g. Hodell et al., 1991) and sedimentation rate in the Siwalik Group, Himalayan foreland basin (Nakayanma and Ulak, 1999), located downstream of the Yarlung Zangbo (which becomes the Tsangpo-Brahmaputra River in India).

5.4. Cenozoic evolution of the India–Asia collision zone

As discussed above, we propose that the Liuqu Conglomerate is a contemporary unit with the Late Oligocene–Miocene Gangrinboche Group (DeCelles et al., 2011), rather than being deposited immediately following Paleocene India–Asia collision or collision between India and an intra-oceanic arc (e.g. Davis et al., 2002; Aitchison et al., 2007; J.G. Wang et al., 2010).

Combining our data with previous studies, we propose general scenarios for the Cenozoic evolution of the India–Asia collision zone. Following India–Asia collision during the Paleocene (e.g. Garzanti et al., 1987; Ding et al., 2005; Najman et al., 2010), uplift of the Lhasa terrane resulted in a continued supply of sediment into basins to the south, and initiated the foreland basin system near the Indus–Yarlung region (e.g. Ding et al., 2005). With the development of Tethyan Himalayan thrust system (Yin, 2006) and accompanying anatexis (Zeng et al., 2011), uplift in the Tethyan Himalaya to the south commenced in Eocene–Oligocene time, and this drove the foreland basin system southward. As convergence continued between the Indian and Asian plates, and with amalgamation of the Tethyan Himalayan and Xigaze basin, upper Oligocene–Miocene conglomerates were successively deposited in local structural depressions along the northern and southern flanks of the Indus–Yarlung suture zone. Firstly, the Qiuwu-Dazhuka conglomerates to the north were derived from the Gangdese belt and Xigaze basin, whereas the younger Liuqu Conglomerate lying to the south was sourced from the Indus–Yarlung suture zone, Lhasa terrane (Xigaze forearc basin) and Tethyan Himalaya (Fig. 7). Ongoing crustal shortening and uplift activated the GCT terminating deposition of the Liuqu Conglomerate and initiating its deformation in the Early Miocene. Subsequently at ~<10–12 Ma, exhumation of the Liuqu Conglomerate commenced (from a paleotemperature of ~90 ± 5 °C) as a result of incision of the Indus–Yarlung suture zone by the ancestral Yarlung Zangbo.

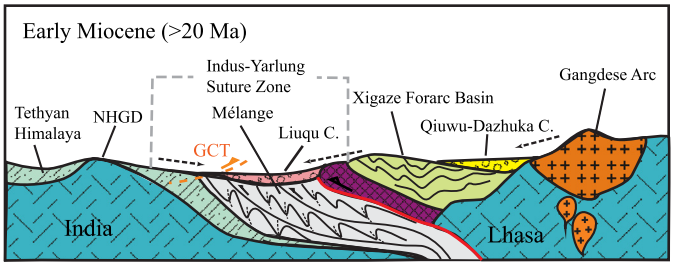

Fig. 7. Tectono-depositional model for the Liuqu Conglomerate in the Early Miocene. Abbreviations: NHGD = Northern Himalaya Gneiss Domes; GCT = Great Counter Thrusts; Liuqu C. = Liuqu Conglomerate; Qiuwu-Dazhuka C. = Qiuwu-Dazhuka Conglomerate.

6. Conclusions

(1) Apatite fission track, apatite and zircon (U–Th)/He data from the Liuqu Conglomerate in the Xigaze area, constrain the timing of deposition of the Liuqu Conglomerate to latest Oligocene–Early Miocene, but probably Early Miocene. Therefore, it should not be considered as a significant stratigraphic marker for constraining any early-stage scenarios for evolution of India–Asia collision.

(2) Combining previous studies, detrital apatite and zircon provenance data presented here suggest that the Liuqu Conglomerate was derived from the Xigaze forearc basin, Indus–Yarlung suture zone, as well as the Tethyan Himalaya.

(3) The pattern of thermal resetting of AFT and AHe data indicates that exhumation of the Liuqu Conglomerate commenced at ~<10–12 Ma (from a paleotemperature of ~90 ± 5 °C) as a result of incision of the Indus–Yarlung suture zone by the ancestral Yarlung Zangbo.

Acknowledgements

Funding for this research was provided by Australia Research Council Discovery Early Career Research Award, DE120102245 (DECRA). The University of Melbourne thermochronology laboratory receives support under the National Collaborative Research Infrastructure AuScope program. We are grateful to Abaz Alimanovic for assistance with ZHe and AHe dating and Jianan Zhao for support during fieldwork. We thank reviewers Barbara Carrapa, Eduardo Garzanti and Editor An Yin for their insightful and constructive comments that helped to improve the manuscript.

Appendix A. Supplementary material

Supplementary material related to this article can be found online at http://dx.doi.org/10.1016/j.epsl.2015.06.010.

References

Aitchison, J.C., Davis, A.M., Badengzhu, Luo, H., 2002. New constraints on the India–Asia collision: the Lower Miocene Gangrinboche conglomerates, Yarlung Tsangpo suture zone, SE Tibet. J. Asian Earth Sci. 21, 251–263. http://dx.doi.org/10.1016/S1367-9120(02)00037-8.

Aitchison, J.C., Ali, J.R., Davis, A.M., 2007. When and where did India and Asia collide? J. Geophys. Res. 112, B05423. http://dx.doi.org/10.1029/2006JB004706.

Allégre, C.J., Courtillot, V., Tapponnier, P., Hirn, A., Mattauer, M., Coulon, C., Jaeger, J.J., Achache, J., Scharer, U., Marcoux, J., Burg, J.P., Girardeau, J., Armijo, R., Gariepy, C., Gopel, C., Li, T., Xiao, X., Chang, C., Li, G., Lin, B., Teng, J., Wang, N., Chen, G., Han, T., Wang, X., Den, W., Sheng, H., Cao, Y., Zhou, J., Qiu, H., Bao, P., Wang, S., Wang, B., Zhou, Y., Xu, R., 1984. Structure and evolution of the Himalaya–Tibet orogenic belt. Nature 307, 17–22. http://dx.doi.org/10.1038/307017a0.

Armstrong, P.A., 2005. Thermochronometers in Sedimentary Basins. In: Reiners, P.W., Ehlers, T.A. (Eds.), Low-temperature thermochronology: Techniques, Interpretations, and Applications. In: Rev. Mineral. Geochem., vol. 58, pp. 499–520.

Brandon, M.T., 1996. Probability density plot for fission-track grain-age samples. Radiat. Meas. 26 (5), 663–676.

Burtner, R.L., Nigrini, A., Donelick, R.A., 1994. Thermochronology of Lower Cretaceous source rocks in the Idaho-Wyoming Thrust Belt. Bull. Am. Assoc. Petrol. Geol. 78, 1613–1636.

Carrapa, B., Orme, D., DeCelles, P.G., Kapp, P., Cosca, M.A., Waldrip, R., 2014. Miocene burial and exhumation of the India–Asia collision zone in southern Tibet, response to slab dynamics and erosion. Geology 42 (5), 443–446. http://dx.doi.org/10.1130/G35350.1.

Dai, J.G., Wang, C.S., Hourigan, J., Li, Z.J., Zhuang, G.S., 2013. Exhumation history of the Gangdese Batholith, southern Tibetan Plateau: evidence from apatite and zircon (U–Th)/He thermochronology. J. Geol. 121 (2), 155–172.

Davis, A.M., Aitchison, J.C., Bai, D.Z., Luo, H., Zyabrev, S., 2002. Paleogene island arc collision-related conglomerates, Yarlung–Tsangpo suture zone, Tibet. Sediment. Geol. 150 (3–4), 247–273.

DeCelles, P.G., Kapp, P., Quade, J., Gehrels, G.E., 2011. Oligocene–Miocene Kailas basin, southwestern Tibet: record of postcollisional upper plate extension in the Indus–Yarlung suture zone. Geol. Soc. Am. Bull. 123, 1337–1362. http://dx.doi.org/10.1130/B30258.1.

DeCelles, P., Kapp, P., Gehrels, G., Ding, L., 2014. Paleocene–Eocene foreland basin evolution in the Himalaya of southern Tibet and Nepal: implications for the age of initial India–Asia collision. Tectonics 33, 824–849. http://dx.doi.org/10.1002/2014TC003522.

Ding, L., Kapp, P., Wan, X., 2005. Paleocene–Eocene record of ophiolite obduction and initial India–Asian collision, south central Tibet. Tectonics 24 (3). http://dx.doi.org/10.1029/2004TC001729. TC3001.

Fang, A.M., Yan, Z., Liu, X.H., Pan, Y.S., Li, J.L., Yu, L.J., Huang, F.X., Tao, J.R., 2006. The age of the plant fossil assemblage in the Liuqu Conglomerate of southern Tibet and its tectonic significance. Prog. Nat. Sci. 16 (1), 55–64.

Farley, K.A., 2002. (U–Th)/He dating: techniques, calibrations, and applications. In: Porcelli, D., Ballentine, C.J., Wieler, R. (Eds.), Noble Gases in Geochemistry and Cosmochemistry. In: Rev. Mineral. Geochem., vol. 47. Mineralogical Society of America, pp. 819–844.

Farley, K.A., Wolf, R.A., Silver, L.T., 1996. The effects of long alpha-stopping distances on (U–Th)/He ages. Geochim. Cosmochim. Acta 60, 4223–4229.

Gansser, A., 1964. Geology of the Himalayas. Interscience Publication, John Wiley and Sons, New York.

Garver, J.I., Brandon, M.T., Roden-Tice, M., Kamp, P.J.J., 1999. Erosional denudation determined by fission-track ages of detrital apatite and zircon. In: Ring, U., Brandon, M.T., Willett, S., Lister, G. (Eds.), Exhumation Processes: Normal Faulting, Ductile Flow, and Erosion. Geol. Soc. (Lond.) Spec. Publ. 154, 283–304.

Garzanti, E., Baud, A., Mascle, G., 1987. Sedimentary record of the northward flight of India and its collision with Eurasia (Ladakh Himalaya, India). Geodin. Acta 1, 297–312.

Gleadow, A., Belton, D.X., Kohn, B.P., Brown, R.W., 2002. Fission track dating of phosphate minerals and the thermochronology of apatite. Rev. Mineral. Geochem. 48, 579–630.

Gleadow, A.J.W., Gleadow, B.P., Belton, S.J., Kohn, D.X., Krochmal, M.S., Brown, R.W., 2009. Coincidence mapping – a key strategy for the automatic counting of fission tracks in natural minerals. Geol. Soc. (Lond.) Spec. Publ. 324 (1), 25–36.

Green, P.F., Duddy, I.R., Gleadow, A.J.W., Tingate, P.R., Laslett, G.M., 1985. Fission track annealing in apatite: track length measurements and the form of the Arrhenius plot. Nucl. Tracks 10, 323–328.

Guo, S.X., 1975. The plant fossils in the Xigaze group of the Mount Everest region. Scientific Survey Report in Mount Everest Region (1966–1968), Paleontology, No. 1. Science Press, Beijing, pp. 411–423 (in Chinese).

Harrison, T.M., Copeland, P., Kidd, W.S., Yin, A., 1992. Raising Tibet. Science 255, 1663–1670. http://dx.doi.org/10.1126/science.255.5052.1663.

Hasebe, N., Barbarand, J., Jarvis, K., Carter, A., Hurford, A.J., 2004. Apatite fission-track chronometry using laser ablation ICP-MS. Chem. Geol. 207 (3–4), 135–145.

Hetzel, R., Dunkl, I., Haider, V., Strobl, M., von Eynatten, H., Ding, L., Frei, D., 2011. Peneplain formation in southern Tibet predates the India–Asia collision and plateau uplift. Geology 39, 983–986. http://dx.doi.org/10.1130/G32069.1.

Hodell, D.A., Mueller, P.A., Garrido, J.R., 1991. Variations in the strontium isotopic composition of seawater during the Neogene. Geology 19, 24–27.

House, M.A., Kohn, B.P., Farley, K.A., Raza, A., 2002. Evaluating thermal history models for the Otway basin, southeastern Australia, using (U–Th)/He and fission-track data from borehole apatites. Tectonophysics 349, 277–295.

Hu, X.M., Wang, J.G., BouDagher-Fadelc, M., Garzantid, E., An, W., 2015. New insights into the timing of the India–Asia collision from the Paleogene Quxia and Jialazi formations of the Xigaze forearc basin, South Tibet. Gondwana Res. http://dx.doi.org/10.1016/j.gr.2015.02.007.

Leary, R., DeCelles, P.G., Quade, J., 2013. The Liuqu Conglomerate: early Miocene basin development related to deformation within the Great Counter Thrust system, southern Tibet. In: American Geophysical Union, Fall Meeting 2013. Abstract, T11A-2420.

Li, G.W., Tian, Y.T., Kohn, B.P., Sandiford, M., Xu, Z.Q., Cai, Z.H., 2015. Cenozoic low temperature cooling history of the Northern Tethyan Himalaya in Zedang, SE Tibet and its implications. Tectonophysics 643, 80–93. http://dx.doi.org/10.1016/j.tecto.2014.12.014.

Ludwig, K.R., 2003. User's Manual for Isoplot 3.0: A Geochronological Toolkit for Microsoft Excel. Spec. Publication, vol. 4. Berkeley Geochronology Center, pp. 1–71.

Najman, Y., Appel, E., Boudagher-Fadel, M., Bown, P., Carter, A., Garzanti, E., Godin, L., Han, J., Liebke, U., Oliver, G., Parrish, R., Vezzoli, G., 2010. Timing of India–Asia collision: geological, biostratigraphic, and palaeomagnetic constraints. J. Geophys. Res. 115, B12416. http://dx.doi.org/10.1029/2010JB007673.

Nakayama, K., Ulak, P.D., 1999. Evolution of fluvial style in the Siwalik Group in the foothills of the Nepal Himalaya. Sediment. Geol. 125 (3), 205–224.

Quidelleur, X., Grove, M., Lovera, O.M., Harrison, T.M., Yin, A., Ryerson, F.J., 1997. Thermal evolution and slip history of the Renbu Zedong Thrust, southeastern Tibet. J. Geophys. Res. 102, 2659–2679.

Reiners, P.W., Spell, T.L., Nicolescu, S., Zanetti, K.A., 2004. Zircon (U–Th)/He thermochronometry: He diffusion and comparisons with $^{40}Ar/^{39}Ar$ dating. Geochim. Cosmochim. Acta 68 (8), 1857–1887.

Rohrmann, A., Kapp, P., Carrapa, B., Reiners, P.W., Guynn, J., Ding, L., Heizler, M., 2012. Thermochronologic evidence for plateau formation in central Tibet by 45 Ma. Geology 40, 187–190.

Tao, J.R., 1998. The Paleogene flora and palaeoclimate of Liuqu formation in Xizang. In: Whyte, P., et al. (Eds.), The Paleoenvironment of East Asia from the Mid-Tertiary. In: Occas. Pap. Monogr. – Cent. Asian Stud., vol. 77. Hong Kong, Centre of Asian Studies, University of Hong Kong, pp. 520–522.

van der Beek, P., Van Melle, J., Guillot, S., Pêcher, A., Reiners, P.W., Nicolescu, S., Latif, M., 2009. Eocene Tibetan plateau remnants preserved in the northwest Himalaya. Nat. Geosci. 2, 364–368. http://dx.doi.org/10.1038/ngeo503.

Wan, X.Q., Sun, L.X., Liu, W.C., Li, G.B., 2007. Stratigraphy of the Yarlung-Tsangpu Suture Zone in Tibet: Beijing. Geological Publishing House, pp. 1–119 (in Chinese).

Wang, A., Garver, J., Wang, G., Smith, J.A., Zhang, K., 2010. Episodic exhumation of the Greater Himalayan Sequence since the Miocene constrained by fission track thermochronology in Nyalam, central Himalaya. Tectonophysics 495, 315–323.

Wang, J.G., Hu, X.M., Garzanti, E., Wu, F., 2013. Upper Oligocene–lower Miocene Gangrinboche Conglomerate in the Xigaze Area, Southern Tibet: implications for Himalayan Uplift and Paleo-Yarlung-Zangbo initiation. J. Geol. 121 (4), 425–444.

Wang, J.G., Hu, X.M., Wu, F.Y., Jansa, L., 2010. Provenance of the Liuqu Conglomerate in southern Tibet: a Paleogene erosional record of the Himalayan–Tibetan orogeny. Sediment. Geol. 231, 74–84. http://dx.doi.org/10.1016/j.sedgeo.2010.09.004.

Wei, L., Liu, X., Yan, FuHua, Mai, XueShun, Li, GuangWei, Liu, XiaoBing, Zhou, X.J., 2011. Palynological evidence sheds new light on the age of the Liuqu Conglomerates in Tibet and its geological significance. Sci. China, Ser. D, Earth Sci. 54 (6), 901–911.

Wolfe, M.R., Stockli, D.F., 2010. Zircon (U–Th)/He thermochronometry in the KTB drill hole, Germany, and its implication for bulk He diffusion kinetics in zircon. Earth Planet. Sci. Lett. 295, 69–82.

Yin, A., 2006. Cenozoic tectonic evolution of the Himalayan orogen as constrained by along strike variation of structural geometry, exhumation history, and foreland sedimentation. Earth-Sci. Rev. 76, 1–131.

Yin, J.X., Suns, X.X., Sun, Y.Y., 1988. Stratigraphy on the Molasse-Type Sediments of the Paired Molasses Belts in the Xigaze Region, South Xizang. Mem. Inst. Geol. Chin. Acad. Sci., vol. 3. Science Press, Beijing, pp. 158–176 (in Chinese).

Zeng, L., Gao, L.E., Xie, K., Liu-Zeng, J., 2011. Mid-Eocene high Sr/Y granites in the Northern Himalayan Gneiss Domes: melting thickened lower continental crust. Earth Planet. Sci. Lett. 303 (3), 251–266.